Reduced modeling of valve dynamics: application to the simulation of cardiac hemodynamics.

COMMEDIA-INRIA Project-Team

Geremy LOACHAMÍN

M2 AMS
2022

Contents

Chapter 1

Introduction

The heart is one of the most important organs because it is responsible for transporting blood throughout the body via the circulatory system, where the opening-closing mechanism plays an important role in ensuring the unidirectional flow of blood (see Fig. 1). Numerical simulation of heart is an important tool in mathematical applications, since its results are intended to serve as a support tool for decision making when studying and understanding this organ and its different pathologies, as well as for the development of implantable devices, but due to its complexity, such simulations present many difficulties, especially because the opening-closing mechanism occurs in very short time intervals.

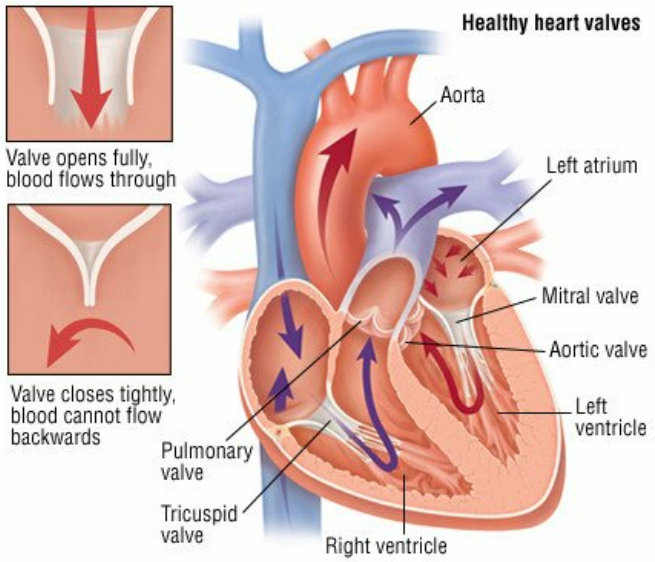

Figure 1.1: Cross-section of the human heart. The upper left part of the diagram shows the opening-closing mechanism of a heart valve. Image from (Anderson 2021).

In particular, the numerical simulation where elastic thin structures such as cardiac valves and incompressible viscous fluids such as blood interact mechanically is known as Fluid-Structure Interaction (FSI) simulation, which has become in recent years an essential tool in the mathematical modeling of the heart. In fact, the first 3D FSI models and simulations of cardiac valves appeared at the beginning of this century (see, e.g., (Hart, Peters, Schreurs, and Baaijens 2003), (Einstein, Kunzelman, Reinhall, Nicosia, and Cochran 2004)), gradually gaining great interest in the academic world.

Despite the great advances achieved, the FSI simulation of cardiac hemodynamics continues to be a rather complex problem, so to overcome such complexity, several simplified alternative models (called reduced models) have been proposed in the literature (see, e.g., (Astorino, Hamers, Shadden, and Gerbeau 2012), (Boilevin-Kayl 2019), (Tagliabue, Dedè, and Quarteroni 2017), (Fedele, Faggiano, Dedè, and Quarteroni 2017)), where the fundamental idea of these approaches is to understand and describe the valve dynamics, whose main advantage is the reduction of computational complexity (see (Sainte-Marie, Chapelle, Cimrman, and Sorine 2006)), but without losing the ability to provide realistic results that allow us to observe the evolution of certain macroscopic quantities such as ventricular and aortic pressures.

Models commonly considered for describing the dynamics of a valve has a complexity that is more in line with the available clinical data. For example, if we consider the cardiac valve as a surface immersed in the fluid, it can be described in a simplified manner by neglecting its dynamics and only considering its open and closed configurations. In fact, in (Astorino, Hamers, Shadden, and Gerbeau 2012) this type of model is studied, where some physiological criteria are used to describe the mechanism of opening and closing of the valve. In addition, a number of 2D and 3D numerical simulations are provided, which allow to appreciate the limitations and properties of this model.

However, simpler and more intuitive models can also be considered. For example, problems subject to unilateral flow constraints involving a nonlinear interface condition written as an inequality and which can even be approximated if we consider unilateral contact problems coming from deformable body mechanics (see, e.g., (Chouly and Hild 2013b), (Chouly, Hild, and Renard 2014)).

Another types of models that can be adapted to describe the dynamics of a valve come from solid mechanics and the numerical implementation of contact and impact problems which generally use the finite element method (FEM) (see (Chouly and Hild 2013a)). There is even a proposal to use a special FEM inspired by Nitsche's method (Nitsche 1971) which allows to treat boundary or interface conditions in a weak sense, thanks to a consistent penalty term.

In particular, we are interested in a model in which, for simplicity, the valve is assumed to be a single interface immersed in the fluid; on this interface we assume constraints that describe in some way the opening-closing mechanism of the valve, which are added to the Navier-Stokes equations describing the blood flow. Thus, the aim of this work is to develop, mathematically study and compare different reduced models that describe valve hemodynamics and reduce the difficulties mentioned above. For this purpose, we consider our study domain around the aortic valve: the left ventricle and a section of the aorta (see Fig. 1.2).

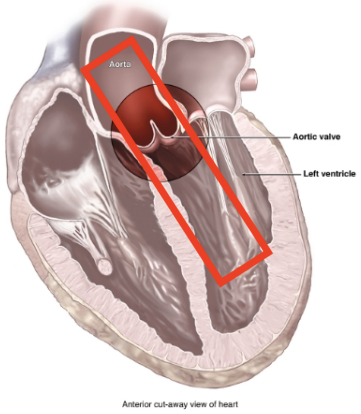

Figure 1.2: Anterior cut-away view of heart. In red, the domain of interest (including the left ventricle, aortic valve and aorta). Image from (Media 2020).

Finally, we have organized this work in four parts. The first chapter corresponds to the Introduction where we briefly present the motivations, problems and the state of the art of this type of reduced models.

In Chapter 2, two reduced models of cardiac valves are introduced: RIS model reported by (Astorino, Hamers, Shadden, and Gerbeau 2012) and a unidirectional flow constraint model. Starting from the ideas proposed by (Astorino, Hamers, Shadden, and Gerbeau 2012) we wrote a more complete model which also includes a term that controls the backflow (see (Arbia, Vignon-Clementel, Hsia, and Gerbeau 2016)). In addition, since the algorithms presented in that work do not consider possible successive changes of the valve status, we include a parameter that avoids these changes and some non-physical vibrations in the pressure. We also propose a modification of the previous RIS model in which the status of the valve changes progressively.

One of the major problems of this model is that it can only be expressed as a discrete time scheme because the changes of state of the valve are performed as long as some physiological criteria are verified. This motivates us to consider another more intuitive model, described as an inequality constraint that ensures unidirectional blood flow across the valve, which is numerically solved using a penalty approach. The resulting problem can be expressed as a time-continuous model, but due to the method used it is not strongly consistent.

In each case, we present their fully-discrete schemes using the conforming stabilized finite element method with an interface-based stabilization allowing the pressure discontinuities through the interface (see (Tobiska and Verfurth 1996)).

In Chapter 3, 2D numerical simulations are performed with FreeFem++, in order to highlight the different properties of these models and to compare them in blood flow regimes. However, as mentioned before, our reduced models also allow us to obtain important information about some macroscopic quantities (such as ventricular and

aortic pressures) which can be represented in a similar way to a Wiggers diagram (see Fig. 1.3). This diagram within cardiac physiology helps to represent and visualize the evolution and behavior of the ventricular (blue) and aortic (red) pressures, and the ventricular volume during a cardiac cycle.

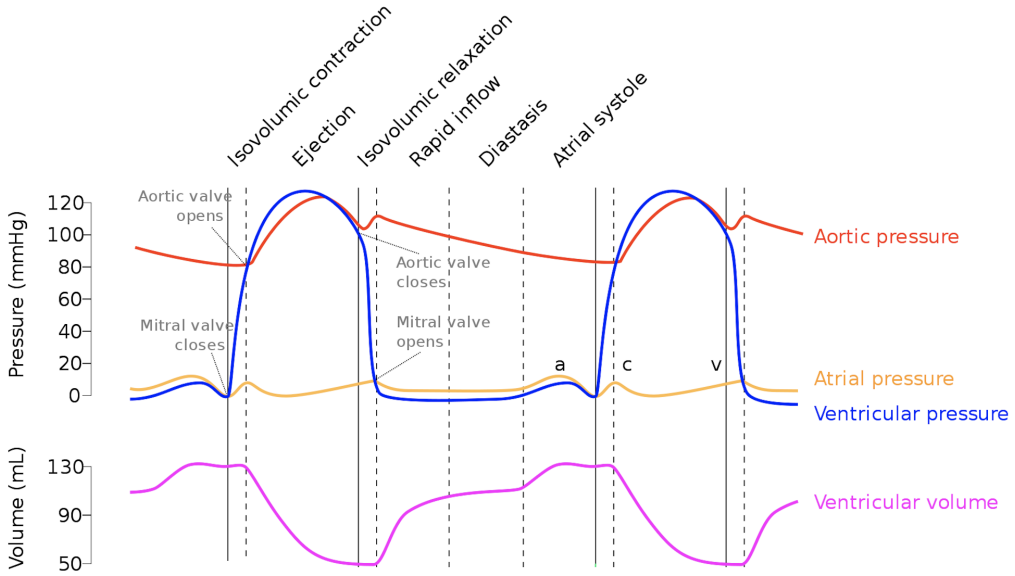

Figure 1.3: Wiggers diagram. Image from (Wikimedia 2020).

Here, we will present two test cases: with the first one we intend to compare the results obtained by (Astorino, Hamers, Shadden, and Gerbeau 2012) with the results obtained from the RIS model proposed in Section 2.2, hoping that they will be quite close; while in the second one we seek to simulate more realistic conditions with which we can have a closer idea of the behavior of the ventricular and aortic pressures. Furthermore, in this context, we seek to observe a physical phenomenon called: blood hammer, which was observed by (Boilevin-Kayl 2019). Blood hammer is a physical phenomenon characterized by an increase in pressure caused when a moving fluid is forced to stop or change direction suddenly.

Conclusions and perspectives are drawn in Chapter 4. In terms of prospects, we propose a model subject to the unilateral boundary conditions that we expect to overcome the limitations of previous models and which is derived using a Nitsche-based method.

Chapter 2

Reduced models for cardiac valves

In this chapter we study of two reduced order models for cardiac valves that describe the opening-closing mechanism of the valve. For each one, we first introduce some notions, notations and important considerations for the models, in Section 2.1. Then, we follow the ideas proposed by (Astorino, Hamers, Shadden, and Gerbeau 2012) to study the RIS model in Section 2.2 which, due to the physiological criterion used to describe the valve dynamics, can only be written as a discrete in time scheme and, a priori, has no continuous equivalent. Finally, in Section 2.3 we propose a model with unidirectional flow constraints on the interface which, unlike the RIS model, can be written as a continuous model in time.

2.1 Preliminary

We that $\Omega \subset \mathbb{R}^d$, with $d = 2, 3$, is a rectangular bounded domain and its boundary is denoted by $\Gamma = \Gamma_D \cup \Gamma_N$, where Γ_D and Γ_N indicate the part of the boundary on which we define homogeneous Dirichlet and non-homogeneous Neumann boundary conditions, respectively. For the sake of simplicity the leaflets are represented by a single interface Σ defined as the intersection between a hyperplane of $\mathbb{R}^d$ and Ω (see Fig. 2.1).

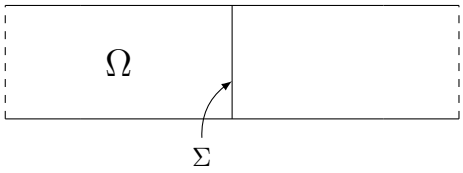

Figure 2.1: The domain Ω and the immersed surface Σ.

Thus, we can decompose the domain Ω in two disjoint connected subdomains Ω_1 and Ω_2 (see Fig. 2.2), which are separated by Σ, *i.e.*,

$$\Omega \setminus \Sigma = \Omega_1 \cup \Omega_2 \qquad \text{and} \qquad \Omega_1 \cap \Omega_2 = \emptyset.$$

Furthermore, we can see the interface Σ as a part of the boundary of each subdomain Ω_i, $i = 1, 2$, which are denoted by $\Gamma_i = \Gamma_{D_i} \cup \Gamma_{N_i} \cup \Sigma$, and where $\Gamma_{D_i} \cup \Gamma_{N_i}$ is the part in common between the boundary Γ and the boundary of each Ω_i. Therefore, Γ_{D_i} and Γ_{N_i} denote the part of Γ_i with homogeneous Dirichlet boundary conditions and a modification of non-homogeneous Neumann boundary conditions[1], respectively.

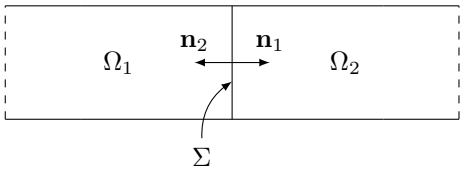

Figure 2.2: The domain Ω decomposed in two subdomains Ω_1 and Ω_2.

We also denote $\mathbf{n}_i$ the unit exterior normal on Γ_i ($i \in \{1, 2\}$). On the interface Σ, we will use the unit exterior normal $\mathbf{n} = \mathbf{n}_1$ as a convention. Thus, for any vector $\mathbf{u} \in \mathbb{R}^d$ its normal component on Σ is defined by $u_n = \mathbf{u} \cdot \mathbf{n}$.

[1] Recall that the non-homogeneous Neumann boundary conditions are defined as $\boldsymbol{\sigma}(\mathbf{u}, p)\mathbf{n} = \mathbf{g}$ on Γ_N. To this condition we add a backflow control term as presented in equation (2.5) and which will be detailed in Remark 2.1

2.2 Resistive immersed surfaces model for cardiac valves (RIS)

In this section, we propose to follow ideas of (Astorino, Hamers, Shadden, and Gerbeau 2012) with some additional considerations such as the introduction of the backflow control term which was introduced in Section 2.2.1. As mentioned earlier, we consider leaflets as a single immersed surface, which in this case is resistive to the blood flow and mimics the behavior of a electric diode. This means that we are going to reduce the dynamics of the valve to only two states: open (where blood flow is allowed to pass) and closed (where blood flow is cut off).

In this way, the idea of RIS model is to describe this opening-closing mechanism of the leaflets, depending on the velocity and pressure of the blood close to the interface. For this purpose a dissipative term is introduced, which also ensures the conservation of momentum equation (**RIS**). This term is a time-dependent resistive parameter, which is zero when the valve is open and large when the valve is closed.

After that, we devote a section to write the temporal and spatial discretization of the model. Finally, we present the numerical algorithms linked to the discrete model, which will be implemented for numerical purposes in Chapter 3.

2.2.1 Problem setting

In order to write our reduced model we assume that blood is an homogeneous incompressible Newtonian fluid, with constant density $\rho > 0$ and constant viscosity $\mu > 0$, governed by the Navier-Stokes equations. So, given $\mathbf{u}^0 = \mathbf{u}^0(\mathbf{x})\colon \Omega \longrightarrow \mathbb{R}^d$ an initial data, $\mathbf{f} = \mathbf{f}(t,\mathbf{x})\colon \mathbb{R}_+ \times \Omega \longrightarrow \mathbb{R}^d$ a body force and $\mathbf{g} = \mathbf{g}(t,\mathbf{x})\colon \mathbb{R}_+ \times \Gamma_N \longrightarrow \mathbb{R}^d$ the body loads, we consider the *Navier-Stokes counterpart problem in a two-domain formulation*: *find a velocity* $\mathbf{u} = \mathbf{u}(t,\mathbf{x})\colon \mathbb{R}_+ \times \Omega \longrightarrow \mathbb{R}^d$ *and a pressure* $p = p(t,\mathbf{x})\colon \mathbb{R}_+ \times \Omega \longrightarrow \mathbb{R}$ *such that*

$$\rho\partial_t \mathbf{u}_i + \rho(\mathbf{u}_i \cdot \nabla)\mathbf{u}_i - \operatorname{div} \boldsymbol{\sigma}(\mathbf{u}_i, p_i) = \mathbf{f}_i \qquad \text{in } [0,T]\times\Omega_i, \quad i=1,2, \tag{2.1}$$

$$\operatorname{div} \mathbf{u}_i = 0 \qquad \text{in } [0,T]\times\Omega_i, \quad i=1,2, \tag{2.2}$$

$$\mathbf{u}_i|_{t=0} = \mathbf{u}_i^0 \qquad \text{in } \Omega_i, \quad i=1,2, \tag{2.3}$$

subject to the following boundary conditions:

$$\mathbf{u}_i = \mathbf{0} \qquad \text{on } [0,T]\times\Gamma_{D_i}, \quad i=1,2, \tag{2.4}$$

$$\boldsymbol{\sigma}(\mathbf{u}_i, p_i)\mathbf{n}_i - \frac{\rho}{2}[\mathbf{u}_i\cdot\mathbf{n}_i]_-\mathbf{u}_i = \mathbf{g}_i \qquad \text{on } [0,T]\times\Gamma_{N_i}, \quad i=1,2, \tag{2.5}$$

and interface conditions:

$$[\![\mathbf{u}]\!] = \mathbf{0} \qquad \text{on } [0,T]\times\Sigma, \tag{2.6}$$

$$[\![\boldsymbol{\sigma}(\mathbf{u},p)\mathbf{n}]\!] = -R_\Sigma \mathbf{u} \qquad \text{on } [0,T]\times\Sigma, \tag{2.7}$$

where $\boldsymbol{\sigma}(\mathbf{u},p) = 2\mu\boldsymbol{\varepsilon}(\mathbf{u}) - p\mathbf{I}$ is the Cauchy stress tensor associated to $\mathbf{u}$ and p, with $\boldsymbol{\varepsilon}(\mathbf{u}) = \frac{1}{2}\big(\nabla\mathbf{u} + \nabla\mathbf{u}^\top\big)$ the strain tensor and $\mathbf{I}$ the identity tensor in $\mathbb{R}^d$. We denote by $\mathbf{u}_i = \mathbf{u}|_{\Omega_i}$, $p_i = p|_{\Omega_i}$, $\mathbf{f}_i = \mathbf{f}|_{\Omega_i}$ and $\mathbf{g}_i = \mathbf{g}|_{\Gamma_{N_i}}$, $i = 1,2$. In addition, the parameter $R_\Sigma \geq 0$ describes the dissipation caused by the interface which will be further specified below and where the terms $[\![\mathbf{u}]\!] = \mathbf{u}_1 - \mathbf{u}_2$ and $[\![\boldsymbol{\sigma}(\mathbf{u},p)\mathbf{n}]\!] = \boldsymbol{\sigma}(\mathbf{u}_1,p_1)\mathbf{n}_1 + \boldsymbol{\sigma}(\mathbf{u}_2,p_2)\mathbf{n}_2$ so defined, denote the velocity jump and the stress jump across the interface Σ, respectively.

In this RIS model, the variation of the resistance R_Σ is described through the physiological criterion presented below in Remark 2.3 and plays an important role in the modeling of a cardiac valve, since it allows describing its dynamics: if the valve resistance is zero ($R_\Sigma = 0$), it means that the valve is open, whereas if the resistance value ($R_\Sigma \neq 0$) is large enough to prevent blood flow, we say that the valve is closed.

Remark 2.1. *Condition (2.5) is a modification of the Neumann boundary condition, which will only be perturbed in the presence of backflow, i.e.,* $-\frac{\rho}{2}[\mathbf{u}_i\cdot\mathbf{n}_i]_-\mathbf{u}_i$ *turns out to be a stabilization term acting only during backflow and where* $[\mathbf{u}_i\cdot\mathbf{n}_i]_-$ *denotes the negative part of the normal velocity in each subdomain. Several backflow control terms have been proposed in the literature, in particular, this choice has been widely employed in hemodynamic regimes (Arbia, Vignon-Clementel, Hsia, and Gerbeau 2016), where energy stability is also ensured. Precisely, this was shown numerically by (Moghadam, Bazilevs, Hsia, Vignon, Marsden, and of Congenital Hearts Alliance 2011).*

Weak formulation

Notation: From now on, we use the standard Lebesgue and Sobolev spaces: $L^2(\Omega)$, $H^1(\Omega)$ and $L^2(\Gamma)$ endowed with their usual norms and scalar products that we denote

$$\begin{aligned} \|\cdot\|_\Omega = \|\cdot\|_{L^2(\Omega)} \qquad \|\cdot\|_{1,\Omega} = \|\cdot\|_{H^1(\Omega)}, \qquad \text{and} \qquad \|\cdot\|_\Gamma = \|\cdot\|_{L^2(\Gamma)}, \\ (\cdot,\cdot)_\Omega = (\cdot,\cdot)_{L^2(\Omega)}, \qquad (\cdot,\cdot)_{1,\Omega} = (\cdot,\cdot)_{H^1(\Omega)}, \qquad \text{and} \qquad (\cdot,\cdot)_\Gamma = (\cdot,\cdot)_{L^2(\Gamma)}. \end{aligned}$$

For the vector-valued functional spaces, we use the same notation for their norms:

$$\|\cdot\|_\Omega = \|\cdot\|_{L^2(\Omega)^d}, \qquad \|\cdot\|_{1,\Omega} = \|\cdot\|_{H^1(\Omega)^d}.$$

Let us introduce the following functional spaces:

$$M = L^2(\Omega) \qquad \text{and} \qquad \mathbf{V} = \left\{ \mathbf{v} \in \left(H^1(\Omega)\right)^d ; \mathbf{v} = \mathbf{0} \text{ on } \Gamma_D \right\},$$

endowed with their usual norms $\|\cdot\|_\Omega$ and $\|\cdot\|_{1,\Omega}$, respectively; and the closed subspace of M,

$$M_0 = L^2_0(\Omega) = \left\{ q \in L^2(\Omega); \int_\Omega q \, d\Omega = 0 \right\}.$$

Let $(\mathbf{v}, q) \in \mathbf{V} \times M_0$ with $\mathbf{v}_i = \mathbf{v}|_{\Omega_i}$ and $q_i = q|_{\Omega_i}$, $i = 1, 2$. If we multiply equation (2.1) by $\mathbf{v}_i$, $i = 1, 2$ and equation (2.2) by q_i, $i = 1, 2$, respectively, and integrate in spatial variable in both subdomains we have

$$\begin{aligned} \rho\left(\partial_t \mathbf{u}_i, \mathbf{v}_i\right)_{\Omega_i} + \rho\left((\mathbf{u}_i \cdot \nabla)\mathbf{u}_i, \mathbf{v}_i\right)_{\Omega_i} - \left(\text{div } \boldsymbol{\sigma}(\mathbf{u}_i, p_i), \mathbf{v}_i\right)_{\Omega_i} &= \left(\mathbf{f}_i, \mathbf{v}_i\right)_{\Omega_i}, \\ \left(\text{div } \mathbf{u}_i, q_i\right)_{\Omega_i} &= 0. \end{aligned}$$

After that, if in the first equation above, we use **Lemma 1** in (Arndt, Braack, and Lube 2016) and the definition of the Cauchy tensor $\boldsymbol{\sigma}$, and integrate by parts we obtain

$$\rho\left(\partial_t \mathbf{u}_i, \mathbf{v}_i\right)_{\Omega_i} + \rho\left((\mathbf{u}_i \cdot \nabla)\mathbf{u}_i + \frac{1}{2}\text{div } \mathbf{u}_i \, \mathbf{u}_i, \mathbf{v}_i\right)_{\Omega_i} + 2\mu\left(\boldsymbol{\varepsilon}(\mathbf{u}_i), \boldsymbol{\varepsilon}(\mathbf{v}_i)\right)_{\Omega_i} - \left(p_i, \text{div } \mathbf{v}_i\right)_{\Omega_i} - \left(\boldsymbol{\sigma}(\mathbf{u}_i, p_i)\mathbf{n}_i, \mathbf{v}_i\right)_{\Gamma_i} = \left(\mathbf{f}_i, \mathbf{v}_i\right)_{\Omega_i}.$$

So, thanks to the boundary conditions (2.4)-(2.5), the interface conditions (2.6)-(2.7) and adding in i we can write the system

$$\begin{cases} \displaystyle\sum_{i=1}^{2} \Big[\rho\left(\partial_t \mathbf{u}_i, \mathbf{v}_i\right)_{\Omega_i} + \rho\left((\mathbf{u}_i \cdot \nabla)\mathbf{u}_i + \frac{1}{2}\text{div } \mathbf{u}_i \, \mathbf{u}_i, \mathbf{v}_i\right)_{\Omega_i} + 2\mu\left(\boldsymbol{\varepsilon}(\mathbf{u}_i), \boldsymbol{\varepsilon}(\mathbf{v}_i)\right)_{\Omega_i} \\ \qquad - \left(p_i, \text{div } \mathbf{v}_i\right)_{\Omega_i} - \left(\mathbf{g}_i + \frac{\rho}{2}[\mathbf{u}_i \cdot \mathbf{n}_i]_- \mathbf{u}_i, \mathbf{v}_i\right)_{\Gamma_{N_i}} + \left(R_\Sigma \mathbf{u}_i, \mathbf{v}_i\right)_\Sigma \Big] &= \displaystyle\sum_{i=1}^{2} \left(\mathbf{f}_i, \mathbf{v}_i\right)_{\Omega_i}, \\ \displaystyle\sum_{i=1}^{2} \left(\text{div } \mathbf{u}_i, q_i\right)_{\Omega_i} &= 0. \end{cases}$$

Finally, we obtain the weak formulation of our problem : *find* $(\mathbf{u}, p) \in \mathbf{V} \times M$ *such that*

$$\textbf{(RIS)} \begin{cases} \rho\left(\partial_t \mathbf{u}, \mathbf{v}\right)_\Omega + \rho\left((\mathbf{u} \cdot \nabla)\mathbf{u} + \frac{1}{2}\text{div } \mathbf{u} \, \mathbf{u}, \mathbf{v}\right)_\Omega - \frac{\rho}{2}\left([u_n]_- \mathbf{u}, \mathbf{v}\right)_{\Gamma_N} + 2\mu\left(\boldsymbol{\varepsilon}(\mathbf{u}), \boldsymbol{\varepsilon}(\mathbf{v})\right)_\Omega \\ \qquad - \left(p, \text{div } \mathbf{v}\right)_\Omega + \left(R_\Sigma \mathbf{u}, \mathbf{v}\right)_\Sigma &= \left(\mathbf{f}, \mathbf{v}\right)_\Omega + \left(\mathbf{g}, \mathbf{v}\right)_{\Gamma_N}, \\ \left(\text{div } \mathbf{u}, q\right)_\Omega &= 0, \end{cases}$$

for all $(\mathbf{v}, q) \in \mathbf{V} \times M$.

2.2.2 Numerical scheme

In the current section we describe a fully-discretization of (**RIS**). First, since RIS model includes a dissipative term depending on time, the time semi-discretization of **(RIS)** is done with an implicit scheme and using the standard first order backward differentiation formula. After that, we present a spatial discretization using the conforming stabilized finite element method with an interface-based stabilization allowing the pressure discontinuities across the interface Σ.

Semi-discretization in time

We begin with a semi-discretization in time of the above (**RIS**) formulation. Precisely, we use the first order backward differentiation formula to approximate the term $\partial_t \mathbf{u}$. Moreover, in order to linearize the convective term and the one associated to the control of the backflow, we consider an semi-implicit discretization in time, while for the dissipative term we use an explicit discretization in time because according to the admissibility criterion given in Remark 2.3 this term is dependent on the velocity and pressure at the previous time step. Thus, the discrete in time problem reads: *for any* $k \geq 1$, *find* $(\mathbf{u}^k, p^k) \in \mathbf{V} \times M$ *such that*

$$\begin{cases} \rho\left(\dfrac{\mathbf{u}^k - \mathbf{u}^{k-1}}{\delta t}, \mathbf{v}\right)_\Omega + \rho\left((\mathbf{u}^{k-1}\cdot\nabla)\mathbf{u}^k + \dfrac{1}{2}\mathrm{div}\ \mathbf{u}^{k-1}\ \mathbf{u}^k, \mathbf{v}\right)_\Omega - \dfrac{\rho}{2}\left([\mathbf{u}^{k-1}\cdot\mathbf{n}]_- \mathbf{u}^k, \mathbf{v}\right)_{\Gamma_N} \\ \qquad +2\mu\left(\boldsymbol{\varepsilon}(\mathbf{u}^k), \boldsymbol{\varepsilon}(\mathbf{v})\right)_\Omega - \left(p^k, \mathrm{div}\ \mathbf{v}\right)_\Omega + \left(R_\Sigma^k \mathbf{u}^k, \mathbf{v}\right)_\Sigma = \left(\mathbf{f}^k, \mathbf{v}\right)_\Omega + \left(\mathbf{g}^k, \mathbf{v}\right)_{\Gamma_N}, \\ \qquad\qquad (\mathrm{div}\ \mathbf{u}^k, q)_\Omega = 0, \end{cases}$$

for all $(\mathbf{v}, q) \in \mathbf{V} \times M$.

Remark 2.2. *In fact, we can see* R_Σ^k *as a penalization parameter associated to the condition* $\mathbf{u}^k = \mathbf{0}$ *on the interface* Σ *and it varies according to the criterion chosen to describe the opening-closing mechanism of the valve. In this way, the criterion consider throughout this section is based on some physiological considerations and depends on the local blood flow information: on velocity and pressure close to the interface. Due to this dependency, these physiological conditions cannot be used in practice continuously in time and must be made explicit in time as follows.*

Remark 2.3 (**Remark 1**, (Astorino, Hamers, Shadden, and Gerbeau 2012))**.** *In the above scheme the following dissipative interface term appears:*

$$\left(R_\Sigma^k \mathbf{u}^k, \mathbf{v}\right)_\Sigma = \int_\Sigma R_\Sigma^k \mathbf{u}^k \cdot \mathbf{v} d\Sigma,$$

where R_Σ^k *depends on the valve status at time* k *and the velocity* $\mathbf{u}^{k-1}$ *and pressure* p^{k-1} *at the previous time* $k-1$ *and takes two values according to the following physiological conditions:*

1. *If the valve is subjected to a positive pressure difference:* $\delta P_\Sigma^{k-1} = \dfrac{1}{|\Sigma|}\displaystyle\int_\Sigma p_1^{k-1} - p_2^{k-1}\ d\Sigma > 0$, *then* $R_\Sigma^k = 0$, *i.e., there is not resistance on* Σ. *This indicates the opening of the valve and blood flows across the valve unidirectionally in the direction* $\mathbf{n}$.
2. *If a flow reversal occurs:* $Q_\Sigma^{k-1} = \displaystyle\int_\Sigma \mathbf{u}^{k-1}\cdot\mathbf{n}\ d\Sigma < 0$, *then* $R_\Sigma^k \neq 0$ *is large enough, and will be fixed later. This means the valve is closed and there is no blood circulation across the valve* ($\mathbf{u}^k = \mathbf{0}$ *on* Σ).

However, according to (Astorino, Hamers, Shadden, and Gerbeau 2012), for practical issues in the above condition 1: instead of calculating the difference of pressures around the interface Σ *as defined before, we consider the difference of the average pressures of both subdomains*

$$\delta P_\Sigma^{k-1} = \frac{1}{|\Omega_1|}\int_{\Omega_1} p_1^{k-1}\ d\Omega - \frac{1}{|\Omega_2|}\int_{\Omega_2} p_2^{k-1}\ d\Omega.$$

Regarding the first statement, the evaluation of δP_Σ *can be used as a test condition for the opening of the valve. Indeed, we know that while* $\delta P_\Sigma < 0$, *the valve is closed; whereas if* $\delta P_\Sigma = 0$, *valve is in the process to be opened provided that there is an increase in* δP_Σ. *In this last state the flow across the valve is still zero and it becomes positive after the opening.*

In contrast, if we consider the second statement we see that Q_Σ *cannot be used as a condition for the opening of the valve because the flow is zero as long as the valve is closed and will not change until its opening. From a physiological point of view the valve is open as long as blood flows in the direction* $\mathbf{n}$. *So, the closure occurs when* $Q_\Sigma < 0$.

Precisely, the above physiological conditions will be used in Section 2.2.3 to write an algorithm that allows switching between open and closed states.

Discretization in space

Let $\mathcal{T}_h$ be a family of triangulations of the domain Ω, where $h = \max_{T\in\mathcal{T}_h} h_T$, with h_T denoting the diameter of the triangle T. We also assume that the family of triangulations $\mathcal{T}_h$ is regular, *i.e.*, there exists $C > 0$ such that for all $T \in T_h$,

$$\frac{h_T}{\rho_T} \leq C,$$

where ρ_T denotes the radius of the inscribed circle in T.

Moreover, as we wish the velocity approximation to be continuous in Ω and the pressure to be discontinuous across the interface Σ, we introduce the following velocity and pressure discrete spaces:

$$\mathbf{V}_h = \{\mathbf{v}_h \in [C(\bar{\Omega})]^2;\ \mathbf{v}_h|_T \in (\mathcal{P}_1(T))^2,\ \forall T \in \mathcal{T}_h \text{ and } \mathbf{v}_h = 0 \text{ in } \Gamma\},$$

and

$$M_h = \{q_h \in M_0;\ q_h|_T \in \mathcal{P}_0(T),\ \forall T \in \mathcal{T}_h\}.$$

We also denote $\mathcal{E}_h$ the set of all interelement boundaries (excluding those on interface Σ) in $\mathcal{T}_h$, *i.e.*, if $E \in \mathcal{E}_h$, then $E = T_1 \cap T_2$, with $T_1, T_2 \in \mathcal{T}_h$.

Thus, the discretization in spatial variable by using finite elements reads as follows: *find* $(\mathbf{u}_h^k, p_h^k) \in \mathbf{V}_h \times M_h$ *such that*

$$\left\{ \begin{array}{rl} \rho\left(\dfrac{\mathbf{u}_h^k - \mathbf{u}_h^{k-1}}{\delta t}, \mathbf{v}_h\right)_\Omega + \rho\left((\mathbf{u}_h^{k-1}\cdot\nabla)\mathbf{u}_h^k + \dfrac{1}{2}\mathrm{div}\ \mathbf{u}_h^{k-1}\ \mathbf{u}_h^k, \mathbf{v}_h\right)_\Omega - \dfrac{\rho}{2}\left([\mathbf{u}_h^{k-1}\cdot\mathbf{n}]_-\mathbf{u}_h^k, \mathbf{v}_h\right)_{\Gamma_N} & \\ +2\mu\left(\boldsymbol{\varepsilon}(\mathbf{u}_h^k), \boldsymbol{\varepsilon}(\mathbf{v}_h)\right)_\Omega - \left(p_h^k, \mathrm{div}\ \mathbf{v}_h\right)_\Omega + \left(R_\Sigma^k\mathbf{u}_h^k, \mathbf{v}_h\right)_\Sigma & = \left(\mathbf{f}_h^k, \mathbf{v}_h\right)_\Omega + \left(\mathbf{g}_h^k, \mathbf{v}_h\right)_{\Gamma_N}, \\ (\mathrm{div}\ \mathbf{u}_h^k, q_h)_\Omega & = 0, \end{array} \right.$$

for all $(\mathbf{v}_h, q_h) \in \mathbf{V}_h \times M_h$.

A stabilized finite element approximation

In order to stabilize the Petrov-Galerkin method applied to the Navier-Stokes equations, we add to our system the following term:

$$S(\mathbf{u}_h^k, p_h^k, \mathbf{v}_h, q_h) = \sum_{T\in\mathcal{T}_h} \xi_T \int_T \left(\mathbf{u}_h^{k-1}\cdot\nabla\right)\mathbf{u}_h^k \cdot \left(\mathbf{u}_h^{k-1}\cdot\nabla\right)\mathbf{v}_h\ d\Omega + \alpha \sum_{E\in\mathcal{E}_h} \frac{h_T}{\mu}\int_E [p_h^k]_E[q_h]_E\ dE = 0, \tag{2.8}$$

where

$$\xi_T = \frac{1}{\rho\sqrt{\dfrac{4}{\delta t^2} + \dfrac{4\left\|\mathbf{u}_h^{k-1}\right\|_{L^2}^2}{h_T^2} + \dfrac{16\mu^2}{h_T^4}}},$$

$\alpha > 0$ and $[q]_E$ denotes the jump of q across $E \in \mathcal{E}_h$ in a fixed direction.

This stabilization $S(\mathbf{u}_h^k, p_h^k, \mathbf{v}_h, q_h)$ is composed of two contributions: a residual based stabilization giving a L^2-control on the convective term, and an interface based stabilization providing L^2-control on the jumps of the pressure (see (Tobiska and Verfurth 1996)).

Hence our fully discrete problem reads: *find* $(\mathbf{u}_h^k, p_h^k) \in \mathbf{V}_h \times M_h$ *such that*

$$\begin{aligned} \rho\left(\frac{\mathbf{u}_h^k - \mathbf{u}_h^{k-1}}{\delta t}, \mathbf{v}_h\right)_\Omega + \rho\left((\mathbf{u}_h^{k-1}\cdot\nabla)\mathbf{u}_h^k + \frac{1}{2}\mathrm{div}\ \mathbf{u}_h^{k-1}\ \mathbf{u}_h^k, \mathbf{v}_h\right)_\Omega - \frac{\rho}{2}\left([u_{h,n}^{k-1}]_-\mathbf{u}_h^k, \mathbf{v}_h\right)_{\Gamma_N} + 2\mu\left(\boldsymbol{\varepsilon}(\mathbf{u}_h^k), \boldsymbol{\varepsilon}(\mathbf{v}_h)\right)_\Omega \\ - \left(p_h^k, \mathrm{div}\ \mathbf{v}_h\right)_\Omega + \left(R_\Sigma^k\mathbf{u}_h^k, \mathbf{v}_h\right)_\Sigma - \left(\mathbf{f}_h^k, \mathbf{v}_h\right)_\Omega - \left(\mathbf{g}_h^k, \mathbf{v}_h\right)_{\Gamma_N} + (\mathrm{div}\ \mathbf{u}_h^k, q_h)_\Omega + S(\mathbf{u}_h^k, p_h^k, \mathbf{v}_h, q_h) = 0, \end{aligned} \tag{2.9}$$

for all $(\mathbf{v}_h, q_h) \in \mathbf{V}_h \times M_h$.

Remark 2.4. *Regarding the numerical analysis of the above discrete problem, for a scheme similar*[2] *to* (2.9)*, its strong consistency is established in* **Theorem 3.2** *(Tobiska and Verfurth 1996) while its existence and uniqueness are shown in* **Remark 3.1** *(Tobiska and Verfurth 1996).*

[2]Derived from the Navier-Stokes equations with Dirichlet boundary conditions using a streamline diffusion finite element method.

2.2.3 Numerical algorithms

Let's start by rewriting as an algorithm the time evolution of the resistance magnitude R_Σ based on the admissibility criterion given in Remark 2.3. Therefore, we recall that if the valve is closed, it will open if there is a positive pressure difference δP_Σ. On the other hand, if the valve is open, it will close if a backflow is detected: $Q_\Sigma < 0$.

In fact, R_Σ takes the values 0 to represent the absence of the interface (the valve is open) and a sufficiently large value $\mathrm{R_{critical}}$ to represent the presence of the interface (it is closed). See **Algorithm 1**.

Algorithm 1: update_resistance

```
1  if(closed_valve == true) then
2      if(δP_Σ > 0) then
3          R_Σ = 0;
4          closed_valve == false;
5      end
6  else
7      if(Q_Σ < 0) then
8          R_Σ = R_critical;
9          closed_valve == true;
10     end
11 end
```

Update of resistance and valve status (open or closed) according to the admissibility criterion considered in Remark 2.3. (Astorino, Hamers, Shadden, and Gerbeau 2012)

Remark 2.5. *In Chapter 3, we also consider a progressive (linear) update for the resistance, i.e., instead of making a sudden switch from zero to* $\mathrm{R}_{critical}$*, we implement a progressive closure where the resistance values increase linearly from 0 to the critical resistance. Similarly, for the opening of the valve, the resistance decreases from* $\mathrm{R}_{critical}$ *to zero (see Fig. 2.3).*

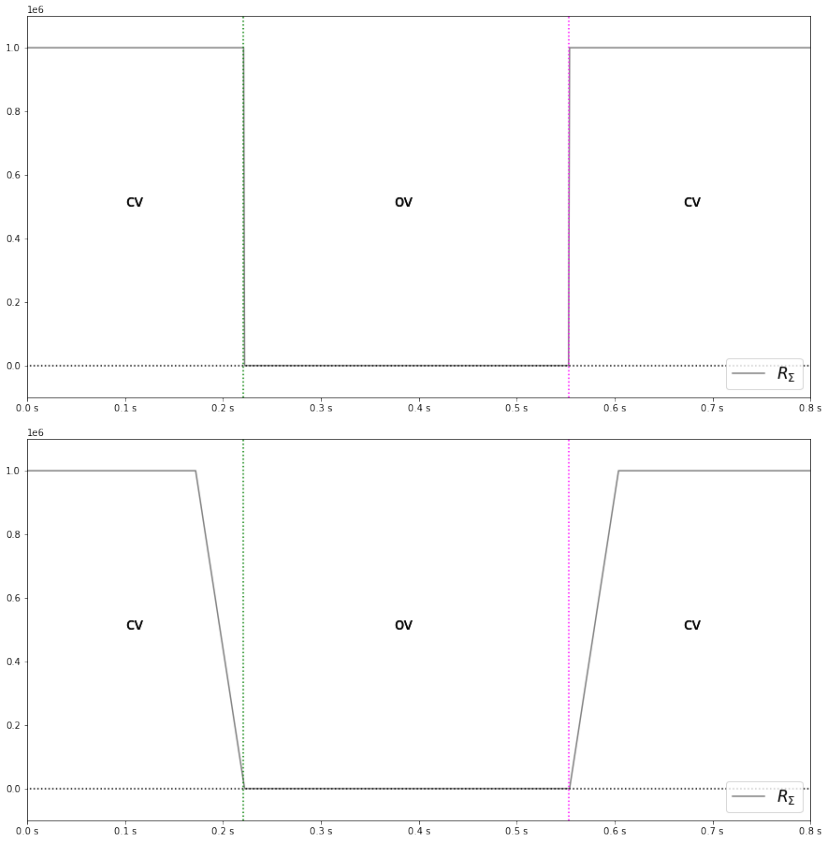

Figure 2.3: Time history of the evolution of the resistance magnitude considering sudden (on the top) and progressive state (on the bottom) switches, where cv and ov denote the status of the valve (closed valve or open valve)

Now, we introduce a routine to check the state of the valve at each time step according to our admissibility criteria presented in Remark 2.3:

Algorithm 2: status_valve

```
if(closed_valve == true) then
    if(δP_Σ > 0) then
        return false;
    end
else
    if(Q_Σ < 0) then
        return false;
    end
end
return true
```

(Astorino, Hamers, Shadden, and Gerbeau 2012)

Remark 2.6. *The following technical consideration is worth mentioning at this point: in the model proposed by (Astorino, Hamers, Shadden, and Gerbeau 2012),* **Algorithm 2** *plays an important role in the switch of state, but in our case, in order to control the time of change from one state to another (open to closed or closed to open), we prevent a new state change for a fixed number of time steps after a state change. For this, a new parameter is added in the above algorithm which indicates the minimum number of iterations that must occur before a state change, this allows us to prevent excessive state changes that can be generated with the original algorithm and may lead to non-realistic oscillations in the status of the valve.*

Recall that in this model, we introduce the dissipative interface term that makes the continuous problem **(RIS)** nonlinear due to the presence of the parameter R_Σ and its behavior subject to the physiological criterion in Remark 2.3 which allows a jump in value when there is a change of state of the valve. Moreover, since the current state of the valve depending on the local fluid dynamic conditions, and resistance is written in terms of the velocity and pressure at the previous time step, we have proposed a linear problem discretized in time and space described in Section 2.2.2. However, this problem introduce a delay in the update of R_Σ and in the opening-closing mechanism. In order to remove this delay we consider the following algorithm:

Algorithm 3: time_advancing_scheme

```
At a time t^k, (u^n, p^n) = (u^k, p^k)
admissible = status_valve(u^k, p^k)
while(admissible == false) do
    R_Σ^n = update_resistance(u^n, p^n) ;
    Solve NS with R_Σ^n;
    admissible = status_valve(u^{k+1}, p^{k+1})
    (u^n, p^n) = (u^{k+1}, p^{k+1})
end
```

(Astorino, Hamers, Shadden, and Gerbeau 2012)

Note that this strategy is computational cheap because we have to recalculate the Navier-Stokes problem only when the valve change of state.

2.3 Constraint model for cardiac valves

As mentioned above the resistive term included in the RIS model can be seen as a penalty term, this motivates to study a little more the penalty method, because unlike the discrete in time scheme written for the RIS model, this method provides us with a continuous model. However, one of the major limitations of the standard penalty method is that it is typically not strongly consistent (Kikuchi and Oden 1988).

2.3.1 Problem setting

In this section we propose to consider the Navier-Stokes problem in a two-domain formulation written in Section 2.2.1 subjected to the following unidirectional *interface condition*:

$$[\![\mathbf{u}]\!] = \mathbf{0} \qquad \text{on } [0,T]\times\Sigma, \tag{2.10}$$

$$u_n \geq 0 \qquad \text{on } [0,T]\times\Sigma. \tag{2.11}$$

Remark 2.7. *In condition (2.11), $u_n \geq 0$ corresponds to an inequality constraint that ensures unidirectional flow in the direction* $\mathbf{n}$*. Moreover, we use u_n instead of $[\![u_n]\!]$ because we apply the continuity condition (2.10).*

Note that the interface conditions are described in terms of inequalities and therefore they cannot be directly applied to numerical calculations. However, for the inequality constraint $u_n \geq 0$, there exists a Lagrange multiplier $\lambda \geq 0$ such that $\lambda u_n = 0$ (complementary slackness). From which we deduce the following weak formulation : *find* $(\mathbf{u}, p) \in \mathbf{V} \times M$ *such that*

$$\textbf{(CM)} \begin{cases} \rho\left(\partial_t \mathbf{u}, \mathbf{v}\right)_\Omega + \rho\left((\mathbf{u}\cdot\nabla)\mathbf{u} + \frac{1}{2}\mathrm{div}\ \mathbf{u}\ \mathbf{u}, \mathbf{v}\right)_\Omega - \frac{\rho}{2}\left([\mathbf{u}\cdot\mathbf{n}]_-\mathbf{u}, \mathbf{v}\right)_{\Gamma_N} + 2\mu\left(\boldsymbol{\varepsilon}(\mathbf{u}), \boldsymbol{\varepsilon}(\mathbf{v})\right)_\Omega \\ \qquad - \left(p, \mathrm{div}\ \mathbf{v}\right)_\Omega - \frac{1}{\gamma}\left([-u_n]_+, v_n\right)_\Sigma = \left(\mathbf{f}, \mathbf{v}\right)_\Omega + \left(\mathbf{g}, \mathbf{v}\right)_{\Gamma_N}, \\ \qquad \left(\mathrm{div}\ \mathbf{u}, q\right)_\Omega = 0, \end{cases}$$

for all $(\mathbf{v}, q) \in \mathbf{V} \times M$.

2.3.2 Numerical scheme

Similar to what was done for the RIS model, we combine an implicit temporal discretization with a spatial discretization using conformal and stable finite elements with an interface-based stabilization. Then, we consider the following fully discrete problem: *for* $k \geq 1$, *find* $(\mathbf{u}_h^k, p_h^k) \in \mathbf{V}_h \times M_h$ *such that*

$$\begin{aligned} &\rho\left(\frac{\mathbf{u}_h^k - \mathbf{u}_h^{k-1}}{\delta t}, \mathbf{v}_h\right)_\Omega + \rho\left((\mathbf{u}_h^{k-1}\cdot\nabla)\mathbf{u}_h^k + \frac{1}{2}\mathrm{div}\ \mathbf{u}_h^{k-1}\ \mathbf{u}_h^k, \mathbf{v}_h\right)_\Omega - \frac{\rho}{2}\left([u_{h,n}^{k-1}]_-\mathbf{u}_h^k, \mathbf{v}_h\right)_{\Gamma_N} + 2\mu\left(\boldsymbol{\varepsilon}(\mathbf{u}_h^k), \boldsymbol{\varepsilon}(\mathbf{v}_h)\right)_\Omega \\ &\quad - \left(p_h^k, \mathrm{div}\ \mathbf{v}_h\right)_\Omega - \frac{1}{\gamma}\left(\left[-u_{h,n}^k\right]_+, v_{h,n}\right)_\Sigma - \left(\mathbf{f}_h^k, \mathbf{v}_h\right)_\Omega - \left(\mathbf{g}_h^k, \mathbf{v}_h\right)_{\Gamma_N} + \left(\mathrm{div}\ \mathbf{u}_h^k, q_h\right)_\Omega + S(\mathbf{u}_h^k, p_h^k, \mathbf{v}_h, q_h) = 0, \end{aligned} \tag{2.12}$$

for all $(\mathbf{v}_h, q_h) \in \mathbf{V}_h \times M_h$. Where S was defined in (2.8).

Remark 2.8. *Let $\gamma > 0$. Thanks to* **Theorem 3** *in (Zhou and Saito 2016), we know that a similar problem*[3] *to the one described in (2.12) admits one unique solution. In addition, the penalty method is not strongly consistent so the reader is referred to* **Section 3.5.** *in (Kikuchi and Oden 1988).*

Newton's Method

We can note that the above discrete formulation is a nonlinear problem due to the penalty term. So, we will proceed to approximate its solution by using the Newton's method. Precisely,we consider $F\colon \mathbf{V}_h \times M_h \longrightarrow \mathbb{R}$ given by

$$\begin{aligned} F\big((\mathbf{u}_h^k, p_h^k)\big) =& \frac{\rho}{\delta t}\left(\mathbf{u}_h^k - \mathbf{u}_h^{k-1}, \mathbf{v}_h\right)_\Omega + \rho\left((\mathbf{u}_h^{k-1}\cdot\nabla)\mathbf{u}_h^k + \frac{1}{2}\mathrm{div}\ \mathbf{u}_h^{k-1}\ \mathbf{u}_h^k, \mathbf{v}_h\right)_\Omega \\ &- \frac{\rho}{2}\left(\left[u_{h,n}^{k-1}\right]_-\mathbf{u}_h^k, \mathbf{v}_h\right)_{\Gamma_N} + 2\mu\left(\boldsymbol{\varepsilon}(\mathbf{u}_h^k), \boldsymbol{\varepsilon}(\mathbf{v}_h)\right)_\Omega - \left(p_h^k, \mathrm{div}\ \mathbf{v}_h\right)_\Omega \\ &- \frac{1}{\gamma}\left(\left[-u_{h,n}^k\right]_+, v_{h,n}\right)_\Sigma - \left(\mathbf{f}_h^k, \mathbf{v}_h\right)_\Omega - \left(\mathbf{g}_h^k, \mathbf{v}_h\right)_{\Gamma_N} + \left(\mathrm{div}\ \mathbf{u}_h^k, q_h\right)_\Omega \\ &+ S(\mathbf{u}_h^k, p_h^k, \mathbf{v}_h, q_h). \end{aligned}$$

Thus, for a fixed time $k \geq 1$, *we look for* $(\mathbf{u}_h^k, p_h^k)$ *such that* $F\big((\mathbf{u}_h^k, p_h^k)\big) = 0$ applying the following algorithm:

Algorithm 4: Newton's Algorithm

Take $(\mathbf{u}_h^{k,0}, p_h^{k,0}) \in \mathbf{V}_h \times M_h$ an initial datum;
for$(j = 0,\ j < \mathrm{Niter};\ j = j + 1)$
  Solve $DF\big((\mathbf{u}_h^{k,j}, p_h^{k,j})\big)(\delta\mathbf{u}_h^{k,j}, \delta p_h^{k,j}) = F\big((\mathbf{u}_h^{k,j}, p_h^{k,j})\big)$;
  $\big(\mathbf{u}_h^{k,j+1}, p_h^{k,j+1}\big) = \big(\mathbf{u}_h^{k,j}, p_h^{k,j}\big) + \big(\delta\mathbf{u}_h^{k,j}, \delta p_h^{k,j}\big)$;
end
  break $\left\|\left(\delta\mathbf{u}_h^{k,j}, \delta p_h^{k,j}\right)\right\|_\Omega < \varepsilon$.

[3] This problem is derived from the Signorini's condition of elasticity theory for a model where the blood vessel is a branched pipe and where artificial boundary conditions are considered on the outflow boundary.

And where the linear application $DF\big((\mathbf{u}_h^{k,j}, p_h^{k,j})\big)$ *is the differential of* F *at point* $(\mathbf{u}_h^{k,j}, p_h^{k,j})$*, given by*

$$\begin{aligned} DF\big((\mathbf{u}_h^{k,j}, p_h^{k,j})\big)(\delta\mathbf{u}_h^{k,j}, \delta p_h^{k,j}) =& \frac{\rho}{\delta t}\left(\delta\mathbf{u}_h^{k,j}, \mathbf{v}_h\right)_\Omega + \rho\left((\mathbf{u}_h^{k-1,j}\cdot\nabla)\delta\mathbf{u}_h^{k,j} + \frac{1}{2}\mathrm{div}\ \mathbf{u}_h^{k-1,j}\ \delta\mathbf{u}_h^{k,j}, \mathbf{v}_h\right)_\Omega \\ &- \frac{\rho}{2}\left(\left[u_{h,n}^{k-1}\right]_-\delta\mathbf{u}_h^{k,j}, \mathbf{v}_h\right)_{\Gamma_N} + 2\mu\left(\boldsymbol{\varepsilon}(\delta\mathbf{u}_h^{k,j}), \boldsymbol{\varepsilon}(\mathbf{v}_h)\right)_\Omega - \left(\delta p_h^{k,j}, \mathrm{div}\ \mathbf{v}_h\right)_\Omega \\ &+ \frac{1}{\gamma}\big(\mathrm{Hev}(-u_{h,n}^{k,j})\ \delta u_{h,n}^{k,j}, v_{h,n}\big)_\Sigma + (\mathrm{div}\ \delta\mathbf{u}_h^{k,j}, q_h)_\Omega + S(\delta\mathbf{u}_h^{k,j}, \delta p_h^{k,j}, \mathbf{v}_h, q_h). \end{aligned}$$

Here,

$$\mathrm{Hev}(x) = \begin{cases} 1, & \text{if } x \geq 0, \\ 0, & \text{otherwise,} \end{cases}$$

corresponds to the Heaviside function, which is an approximation of the derivate of $[\ \cdot\ ]_+$.

Remark 2.9. *As it is well known, the penalty method is not consistent (Kikuchi and Oden 1988), then we propose another model using a Nitsche-based method proposed by (Chouly and Hild 2013a) which will be detailed in Chapter 4. As mentioned, the latter method has been applied to problems involving conditions in the interface between subdomains, which are treated by a consistent penalty term. This allows us to write a consistent model.*

Chapter 3

Numerical experiments

Throughout this chapter we carry out several numerical simulations the reduced models introduced in the previous chapter. In Section 3.1 under the same conditions proposed by (Astorino, Hamers, Shadden, and Gerbeau 2012), we solve the numerical scheme associated with the RIS model using FreeFem++ (see Fig. 3.1) and the results obtained are compared with their results. In this way, we are able to observe the properties of our models without the aim of providing physiologically relevant numerical simulations. In Section 3.2, we propose to recreate numerically realistic conditions under which we will solve and simulate our reduced models hoping to observe the physical phenomenon: blood hammer. Recall that this phenomenon occurs when a valve closes suddenly producing a pressure wave that propagates inside the vessel.

Figure 3.1: 2D simulation of an open (top) and closed (bottom) valve using FreeFem++.

3.1 First test case: A comparison with RIS model in (Astorino, Hamers, Shadden, and Gerbeau 2012)

In this first test case, we consider a simple rigid rectangle with an interface in the middle. The computational domain is given in Fig. 3.1. For all the test cases, we also consider the following values for the fluid density $\rho = 1.0\ g/cm^3$ and the fluid viscosity $\mu = 0.035\ g/cm/s$, which are the ones usually set for the blood considered as a Newtonian fluid. The fluid is assumed to be at rest initially, and a sinusoidal pressure is imposed on the inlet boundary

$$\boldsymbol{\sigma}(\mathbf{u}, p)\mathbf{n} - \frac{\rho}{2}[\mathbf{u}\cdot\mathbf{n}]_-\mathbf{u} = -2000\sin(4\pi t)\mathbf{n}.$$

On the outlet boundary, we consider the following condition

$$\boldsymbol{\sigma}(\mathbf{u}, p)\mathbf{n} - \frac{\rho}{2}[\mathbf{u}\cdot\mathbf{n}]_-\mathbf{u} = -P_{rcr}\mathbf{n},$$

where P_{rcr} is given by the Windkessel resistor–capacitor–resistor (RCR) model described by the ODE (see (Vignon-Clementel 2006)):

$$P_{rcr} + R_d\, C\frac{dP_{rcr}}{dt} = (R_p + R_d)Q + R_pR_d\, C\frac{dQ}{dt} + P_d + R_d\, C\frac{dP_d}{dt},$$

where R_p is the proximal resistance, R_d is the distal resistance, C is the capacitance, and P_d is the distal pressure. These parameters are given by $R_p = 150 dyn\cdot s/cm^5$, $R_d = 700 dyn\cdot s/cm^5$, $C = 10^{-3} cm^5/dyn$, and $P_d = 0$.

The simulation is carried out for $1.1s$ with a time step of $5\times 10^{-3}s$. A quantitative representation of the pressure and flow magnitudes across the interface is reported in Fig. 3.3. The blue curve represents the average pressure in Ω_1 and the red one in Ω_2. In addition, non-negative flows across the valve correspond to its opening (ov) and closure (cv) periods.

Then, it is interesting to note that just after the valve closes, a slight increase in pressure is experienced Ω_1. This is the result of two combined effects: the sudden closure of the valve, which depends on the model considered, and the inertia of the fluid. The sudden valve closure and the corresponding discontinuity introduced in the flow are limitations of the RIS model, and may affect the applicability of the model for very small time-steps.

We can see a slight peak in the flow curve that occurs after the valve closes, such behavior was not observed in the results obtained by (Astorino, Hamers, Shadden, and Gerbeau 2012), and may be linked to the conditions considered in the outlet boundary. Moreover, as we can be seen in Fig. 3.3, the results we have obtained are quite similar and consistent, which is indicative of the good performance of our model.

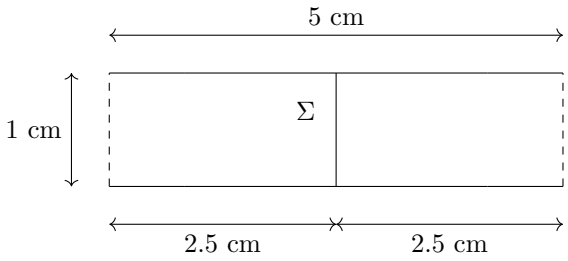

Figure 3.2: The computational domain Ω with the resistive immersed surface Σ.

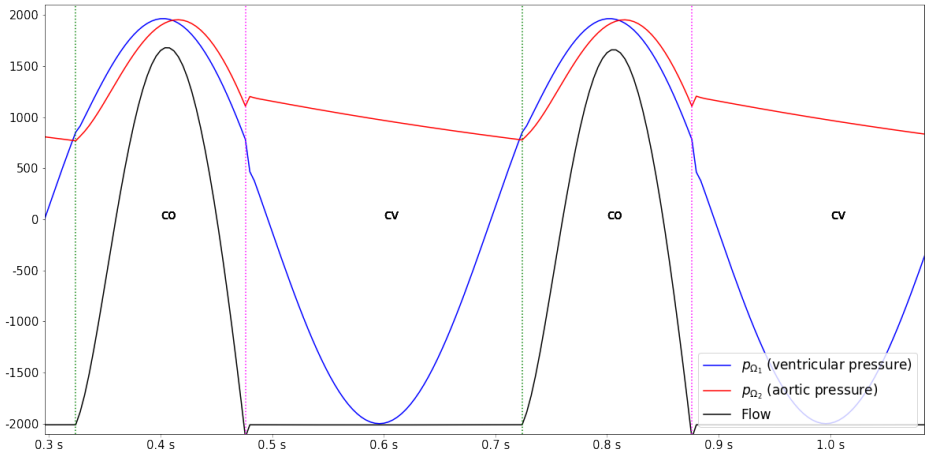

Figure 3.3: Average pressures and flow on the resistive immersed surface in the two subdomains, obtained from the RIS model.

3.2 Second test case: A realistic case

Now, the idea is to recreate the most realistic possible context of a hemodynamic regimen. Thus, we consider Ω as rectangular domain whose dimensions are 10 cm length and 2 cm width with a interface immersed Σ on the middle of this domain (see Fig. 3.2).

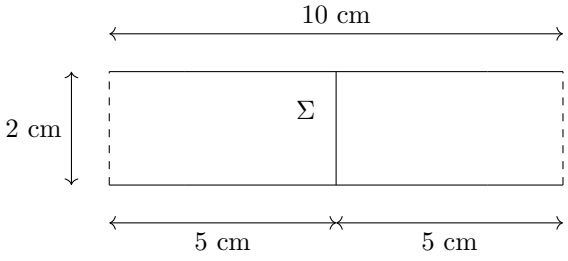

Figure 3.4: The domain Ω and its dimensions.

We suppose that the fluid is initially at rest, and an imposed pressure in the inlet

$$\boldsymbol{\sigma}(\mathbf{u},p)\mathbf{n} - \frac{\rho}{2}[\mathbf{u}\cdot\mathbf{n}]_{-}\mathbf{u} = -\bar{p}_{inlet}(t)\mathbf{n},$$

where $\bar{p}_{inlet}(t)$ corresponds to the ventricular pressure which varies between 0 dyn/cm^2 and 159 960 dyn/cm^2 (systolic pressure). On the outlet, the boundary condition

$$\boldsymbol{\sigma}(\mathbf{u},p)\mathbf{n} - \frac{\rho}{2}[\mathbf{u}\cdot\mathbf{n}]_{-}\mathbf{u} = -\left(\bar{p}_{outlet}(t) + R\int_{\Gamma_{\text{outlet}}} \mathbf{u}\cdot\mathbf{n}\, d\Gamma\right)\mathbf{n}$$

is imposed, where $\bar{p}_{outlet}(t) = 106\ 640\ dyn/cm^2$ is a value that corresponds to the diastolic pressure and $R = 15\ dyn\cdot s/cm^5$ is a resistance. Both quantities are prescribed constants that allow to control the pressure on the outlet.

The simulations are carried out for a total time of $t = 1.1$ s with a time-step 10^{-3}. The whole computational domain Ω is made of 8 000 triangles.

Remark 3.1. *We recall for the in RIS model, since R_Σ corresponds to the interface resistance, it takes the values 0 to represent the absence of the interface (the valve is open) and a sufficiently large value when the interface does not allow that the flow across the valve (it is closed). Hence, we consider a critical resistance $R_{critical}$ large enough such that the flow across the interface is negligible. As well as in (Astorino, Hamers, Shadden, and Gerbeau 2012), we will take $R_{critical} = 10^6$, because in similar simulations using this value it can be ensured that the backflow is no more than 1% of the total flow.*

Results

In the following, by using FreeFem++ to solve the numerical schemes described in Sections 2.2.2 and 2.3.2, we present the mean pressures obtained in both subdomains (Ω_1 and Ω_2) over time, these results correspond to the ventricular (blue) and aortic (red) pressures, respectively, which are represented at the top of the Wiggers diagram (see Fig. 1.3).

RIS model: As mentioned in the previous chapter, it is necessary to add a new parameter which indicates the minimum number of iterations that must occur before a change of the status valve, this helps to prevent successive state changes and non-realistic oscillations in the status of the valve. Thus, in the first Fig. 3.5, the pressure calculated through the RIS model presents an unusual small jump due to the sudden valve closure characteristic of this model and the inertia of the fluid.

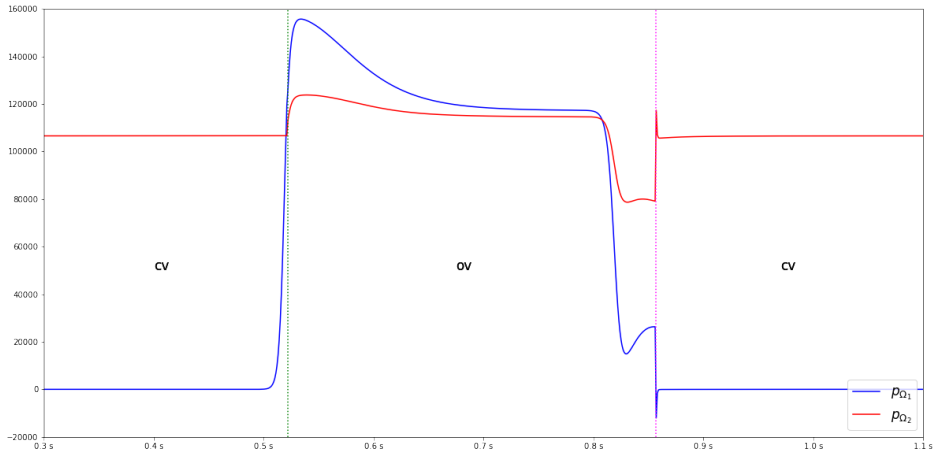

Figure 3.5: Time history of the average pressures (dyn/cm^2) of the two subdomains, obtained from the RIS model.

RIS model with a progressive update resistance: In this case, we consider a progressive change to switch from one state to another. In order to implement this variation of the above scheme, we add a constant parameter in **Algorithm 1** that allows us to control the number of time steps in which the progressive change of the valve status is performed. We see that the results obtained have a better behavior as the jumps observed in the original model (see Fig. 3.5) caused by sudden changes of the valve state are reduced, and now we observe a smoother behavior both in the closing and in the opening of the valve. (see Fig. 3.6).

Constraint model: In the results obtained when using the model with constraints applying the penalty method (see Fig. 3.7), as expected a smoother behavior is observed even in open and closed states, where there is no presence of unusual jumps in pressure.

As we can see, the ventricular (blue) and aortic (red) pressure curves describe a behavior in accordance with the Wiggers diagram and consistent with cardiac dynamics. For example, in the case of aortic pressure, we can see a slight peak after valve closure as observed by (Astorino, Hamers, Shadden, and Gerbeau 2012).

Furthermore, we see that the ventricular pressure varies between 0 dyn/cm^2 and a maximum of 160 000 dyn/cm^2 or about 120 $mmHg$, except for the first model in which after the valve is closed, this pressure takes a negative value. Likewise, we have that the aortic pressure stays around 100 000 dyn/cm^2 or approximately 80 $mmHg$.

Although we see an improvement in the smoothness of the pressure curves when we consider the progressive RIS model and the constrained model, these results are not conclusive as to whether one model is better than the other.

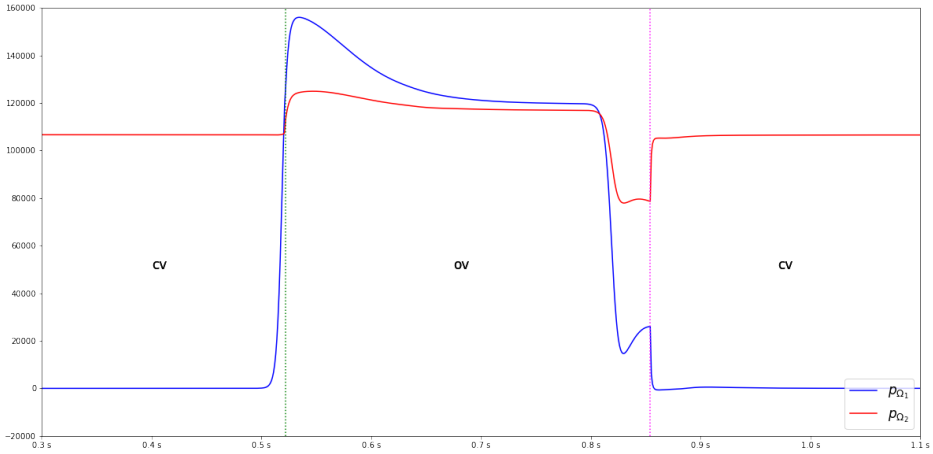

Figure 3.6: Time history of the average pressures (dyn/cm^2) of the two subdomains, obtained from the RIS model with a progressive state switch.

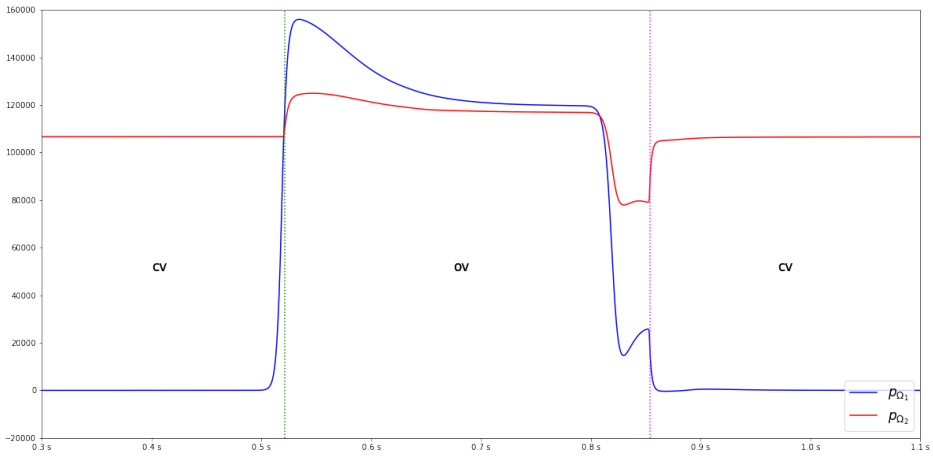

Figure 3.7: Time history of the average pressures (dyn/cm^2) of the two subdomains, obtained from the Constraint model.

Evidently, the RIS model allows us to obtain a linear scheme that when solved requires a lower computational cost than when we solve the scheme coming from the constrained model which, as mentioned in the previous chapter, corresponds to a non-linear problem and for which we use Newton's algorithm.

Chapter 4

Conclusions and Perspectives

Because of its simplicity, the two methods considered in this work present some numerical limitations. In the case of the *RIS model*, we saw that due to the physiological conditions describing opening-closing mechanism of the valve, we can describe this model only through a discrete in time scheme. If instead, we apply the penalty method for our *constrained model*, it can be described continuously in time. However, penalty method is not consistent (Kikuchi and Oden 1988). This motivates us to look for other models that do not present such limitations. Thus, we consider a model with unilateral interface conditions for which we apply a Nitsche-based method which, as we will see below, can be described continuously in time and is also consistent.

Concerning numerical simulations presented in Section 3.2, it was not possible to observe the phenomenon called blood hammer, which can generate strong vibrations when closing and opening the valve. However, we suspect that this physical phenomenon may be linked to a more complex model where the velocity of the structure is also taken into account (see (Boilevin-Kayl 2019)).

Perspectives: Nitsche-based method

Now, we briefly describe a Nitsche-based method. Thus, the first thing we do is to adapt the ideas proposed by (Chouly and Hild 2013a), which were written for an elasticity problem, for a hemodynamic regime.

Precisely, instead of using the interface conditions of the RIS model or the constraint model, we consider the following unilateral (Signorini's type) interface conditions on Σ:

$$u_n \geq 0, \tag{4.1}$$
$$[\![\sigma_n(\mathbf{u},p)]\!] \geq 0, \tag{4.2}$$
$$[\![\sigma_n(\mathbf{u},p)]\!]\, u_n = 0, \tag{4.3}$$
$$[\![\boldsymbol{\sigma}_{\mathbf{t}}(\mathbf{u})]\!] = \mathbf{0}, \tag{4.4}$$

where $\sigma_n(\mathbf{u},p) = (\boldsymbol{\sigma}(\mathbf{u},p)\mathbf{n})\cdot\mathbf{n}$ denotes the normal component of the vector $\boldsymbol{\sigma}(\mathbf{u},p)\mathbf{n}$ while $\boldsymbol{\sigma}_{\mathbf{t}}(\mathbf{u})$ denotes its tangential component, *i.e.*, $\boldsymbol{\sigma}_{\mathbf{t}}(\mathbf{u}) = \boldsymbol{\sigma}(\mathbf{u},p)\mathbf{n} - \sigma_n(\mathbf{u},p)\mathbf{n}$.

Remark 4.1. *The unilateral Signorini's type boundary conditions describe the interaction without friction between the interface and the fluid on Σ. These ones are used instead of the interface conditions considered in the previous sections. More precisely, (4.1)-(4.3) are nonlinear conditions describing unilateral contact on Σ, whereas (4.4) corresponds to the frictionless condition.*

Remark 4.2. *Note that the term $[\![\sigma_n(\mathbf{u},p)\mathbf{n}]\!]$ can be seen as the Lagrange multiplier associated to the condition $u_n \geq 0$, whereas (4.3) would be the complementary slackness.*

Analogously to what was done for the RIS model in Section 2.2.1, we can deduce the variational formulation of the Navier-Stokes counterpart problem in a two-domain formulation subject to the unilateral Signorini's type constraint (4.1)-(4.4). Additionally, we can rewrite this formulation, making use of Proposition 4.1. Thus, our problem reads: *find* $(\mathbf{u},p)\in\mathbf{V}\times M$ *such that*

$$\textbf{(NM)}\quad \begin{cases} \rho\left(\partial_t\mathbf{u},\mathbf{v}\right)_\Omega + \rho\left(\left(\mathbf{u}\cdot\nabla\right)\mathbf{u} + \frac{1}{2}\mathrm{div}\ \mathbf{u}\ \mathbf{u},\mathbf{v}\right)_\Omega - \frac{\rho}{2}\left([\mathbf{u}\cdot\mathbf{n}]_-\mathbf{u},\mathbf{v}\right)_{\Gamma_N} + 2\mu\left(\boldsymbol{\varepsilon}(\mathbf{u}),\boldsymbol{\varepsilon}(\mathbf{v})\right)_\Omega \\ \qquad - \left(p,\mathrm{div}\ \mathbf{v}\right)_\Omega - \frac{\gamma_0}{h}\left(\left[\frac{h}{\gamma_0}[\![\sigma_n(\mathbf{u},p)]\!] - u_n\right]_+, v_n\right)_\Sigma = \left(\mathbf{f},\mathbf{v}\right)_\Omega + \left(\mathbf{g},\mathbf{v}\right)_{\Gamma_N}, \\ \qquad\qquad \left(\mathrm{div}\ \mathbf{u},q\right)_\Omega = 0, \end{cases}$$

for all $(\mathbf{v}, q) \in \mathbf{V} \times M$ and $\gamma_0 > 0$.

Numerical scheme: As for the model with unidirectional flow constraints, the discrete scheme deduced above corresponds to a nonlinear problem whose solution will be approximated using Newton's method. Fully-discrete problem reads as follows: *for* $k \geq 1$*, we look for* $(\mathbf{u}_h^k, p_h^k) \in \mathbf{V}_h \times M_h$ *such that*

$$\begin{aligned} &\frac{\rho}{\delta t}\left(\mathbf{u}_h^k - \mathbf{u}_h^{k-1}, \mathbf{v}_h\right)_\Omega + \rho\left((\mathbf{u}_h^{k-1}\cdot\nabla)\mathbf{u}_h^k + \frac{1}{2}\text{div }\mathbf{u}_h^{k-1}\ \mathbf{u}_h^k, \mathbf{v}_h\right)_\Omega - \frac{\rho}{2}\left(\left[u_{h,n}^{k-1}\right]_-\mathbf{u}_h^k, \mathbf{v}_h\right)_{\Gamma_N} \\ &+2\mu\left(\boldsymbol{\varepsilon}(\mathbf{u}_h^k), \boldsymbol{\varepsilon}(\mathbf{v}_h)\right)_\Omega - \left(p_h^k, \text{div }\mathbf{v}_h\right)_\Omega - \frac{\gamma_0}{h}\left(\left[\frac{h}{\gamma_0}[\![\sigma_n(\mathbf{u}_h^k, p_h^k)]\!] - u_{h,n}^k\right]_+, v_{h,n}\right)_\Sigma - \left(\mathbf{f}_h^k, \mathbf{v}_h\right)_\Omega \\ &- \left(\mathbf{g}_h^k, \mathbf{v}_h\right)_{\Gamma_N} + (\text{div }\mathbf{u}_h^k, q_h)_\Omega + S(\mathbf{u}_h^k, p_h^k, \mathbf{v}_h, q_h) = 0, \end{aligned} \tag{4.5}$$

for all $(\mathbf{v}_h, q_h) \in \mathbf{V}_h \times M_h$.

Moreover, let $\gamma_0 > 0$ enough small, the well-posedness of a discrete formulation similar to the one in (4.5) is shown in **Theorem 3.4.** in (Chouly, Hild, and Renard 2014), while the consistency of this method is dealt with in **Lemma 3.1.** in (Chouly, Hild, and Renard 2014).

With regard to the numerical results that one can obtain with the latter model, we expect to improve their accuracy and to reduce the occurrence of some physical phenomena that can occur due to the sudden change of the valve state and that may disturb the results. However, when considering stress jumps in our interface condition Proposition 4.1, the computational cost can also increase.

Appendix A: The Nitsche-based method

Notation: We introduce the notation $[\,\cdot\,]_+$ for the positive part of $a \in \mathbb{R}$, which is defined as follows

$$[a]_+ = \begin{cases} a, & \text{if } a > 0, \\ 0, & \text{otherwise,} \end{cases}$$

and it verifies: $a \leq [a]_+$ and $[a]_+ a = [a]_+^2$, for all $a \in \mathbb{R}$.

Remark 4.3. *Another useful property of* $[\,\cdot\,]_+$ *that we will invoke later is the following:*

$$([a]_+ - [b]_+)(a-b) \geq 0, \qquad \textit{for all } a,\ b \in \mathbb{R}.$$

Indeed,

$$\begin{aligned} ([a]_+ - [b]_+)(a-b) &= [a]_+ a + [b]_+ b - [b]_+ a - [a]_+ b \\ &\geq [a]_+^2 + [b]_+^2 - 2[b]_+[a]_+ \\ &= ([a]_+ - [b]_+)^2 \geq 0. \end{aligned}$$

Proposition 4.1. *Let* $\gamma_0 > 0$. *The conditions* (4.1)-(4.3) *on* Σ *are equivalents to write*

$$[\![\sigma_n(\mathbf{u},p)]\!] = \frac{\gamma_0}{h}\left[\, \frac{h}{\gamma_0}[\![\sigma_n(\mathbf{u},p)]\!] - u_n \,\right]_+ .$$

Proof. Let $\mathbf{u}$ smooth enough defined in Ω verifying (4.1)-(4.3). We can study the condition (4.2) in two cases:

If $[\![\sigma_n(\mathbf{u},p)]\!] = 0$: by condition (4.1) we know that $u_n \geq 0$, which implies $[-u_n]_+ = 0$. Then,

$$0 = \frac{\gamma_0}{h}\,[-u_n]_+ = [\![\sigma_n(\mathbf{u},p)]\!].$$

If $[\![\sigma_n(\mathbf{u},p)]\!] > 0$: from condition (4.3) we can deduce $u_n = 0$. Then,

$$\frac{\gamma_0}{h}\left[\, \frac{h}{\gamma_0}[\![\sigma_n(\mathbf{u},p)]\!] \,\right]_+ = [\![\sigma_n(\mathbf{u},p)]\!],$$

because $\gamma_0 > 0$.

On the other hand, let $\mathbf{u}$ smooth enough defined in Ω such that

$$[\![\sigma_n(\mathbf{u},p)]\!] = \frac{\gamma_0}{h}\left[\, \frac{h}{\gamma_0}[\![\sigma_n(\mathbf{u},p)]\!] - u_n \,\right]_+ . \tag{4.6}$$

Since $\left[\, \frac{h}{\gamma_0}[\![\sigma_n(\mathbf{u},p)]\!] - u_n \,\right]_+ \geq 0$ and $\gamma_0 > 0$, we have $[\![\sigma_n(\mathbf{u},p)]\!] \geq 0$, *i.e.*, (4.2) holds. Thanks to this condition, from equation (4.6), if $[\![\sigma_n(\mathbf{u},p)]\!] = 0$ we can deduce that $[-u_n]_+ = 0$, which implies $u_n \geq 0$. Moreover, $[\![\sigma_n(\mathbf{u},p)]\!] u_n = 0$. So, (4.1) and (4.3) are verified.

If $[\![\sigma_n(\mathbf{u},p)]\!] > 0$, from equation (4.6) we have $\left[\, \frac{h}{\gamma_0}[\![\sigma_n(\mathbf{u},p)]\!] - u_n \,\right]_+ > 0$. Hence,

$$\frac{h}{\gamma_0}[\![\sigma_n(\mathbf{u},p)]\!] = \left[\, \frac{h}{\gamma_0}[\![\sigma_n(\mathbf{u},p)]\!] - u_n \,\right]_+ = \frac{h}{\gamma_0}[\![\sigma_n(\mathbf{u},p)]\!] - u_n,$$

from where we obtain $u_n = 0$, which implies that the conditions (4.1) and (4.3) are verified. □

Bibliography

Anderson, L. A. (2021). Heart valve problems. https://www.drugs.com/health-guide/heart-valve-problems.html.

Arbia, G., I. Vignon-Clementel, T.-Y. Hsia, and J.-F. Gerbeau (2016). Modified Navier-Stokes equations for the outflow boundary conditions in hemodynamics. *European Journal of Mechanics-B/Fluids 60*, 175–188.

Arndt, D., M. Braack, and G. Lube (2016). Finite elements for the Navier-Stokes problem with outflow condition. *Springer International Publishing 112*, 95–103.

Astorino, M., J. Hamers, S. Shadden, and J.-F. Gerbeau (2012). A robust and efficient valve model based on resistive immersed surfaces. *John Wiley and Sons, Ltd. 28*, 937–959.

Bazilevs, Y., J. Gohean, T. Hughes, R. Moser, and Y. Zhang (2009). Patient-specific isogeometric fluid- structure interaction analysis of thoracic aortic blood flow due to implantation of the Jarvik 2000 left ventricular assist device. *Comput. Methods Appl. Mech. Engrg 198*, 3534–3550.

Boilevin-Kayl, L. (2019). Modeling and numerical simulation of implantable cardiovascular devices, PhD Thesis, Sorbonne Université. *Numerical Analysis. Sorbonne Université*.

Brezis, H. (2011). *Functional Analysis, Sobolev Spaces and Partial Differential Equations* (primera ed.). Universitext. Nueva York, Springer.

Chnafa, C., S. Mendez, and F. Nicoud (2014). Image-based large-eddy simulation in a realistic left heart. *Comp. and Fluids 94*, 173–187.

Chouly, F. and P. Hild (2013a). A Nitsche-based method for unilateral contact problems: numerical analysis. *SIAM Journal on Numerical Analysis, Society for Industrial and Applied Mathematics 51*, 1295–1307.

Chouly, F. and P. Hild (2013b). On convergence of the penalty method for unilateral contact problems. *Applied Numerical Mathematics, Elsevier 65*, 27–40.

Chouly, F., P. Hild, and Y. Renard (2014). Symmetric and non-symmetric variants of Nitsche's method for contact problems in elasticity: theory and numerical experiments. *Mathematics of Computation 84*, 1089–1112.

Einstein, D., K. Kunzelman, P. Reinhall, M. Nicosia, and R. Cochran (2004). Hemodynamic determinants of the mitral valve closure sound: a finite element study. *Med. Biol. Eng. Comput. 42(6)*, 832–846.

Fedele, M., E. Faggiano, L. Dedè, and A. Quarteroni (2017). A patient-specific aortic valve model based on moving resistive immersed implicit surfaces. *Biomech. Model. Mechanobiol 16*, 1779–1803.

Fernández, M., J. Gerbeau, and V. Martin (2008). Numerical simulation of blood flows through a porous interface. *ESAIM: Mathematical Modelling and Numerical Analysis 42*, 961–990.

Girault, V. and P.-A. Raviart (1986). *Finite element methods for Navier-Stokes equations - Theory and algorithms*, Volume 5.

Hart, J. D., G. Peters, P. Schreurs, and F. Baaijens (2003). A three- dimensional computational analysis of fluid-structure interaction in the aortic valve. *J. Biomech. 36(1)*, 103–112.

Hild, P. and Y. Renard (2010). *A stabilized Lagrange multiplier method for the finite element approximation of contact problems in elastostatics*, Volume 115. Numer. Math.

Kikuchi, N. and J. T. Oden (1988). *Contact problems in elasticity: a study of variational inequalities and finite element methods*, Volume 8. SIAM Studies in Applied Mathematics.

Media, N. M. (2020). Bicuspid aortic valve with endocarditis. //catalog.nucleusmedicalmedia.com/bicuspid-aortic-valve-with-endocarditis/view-item?ItemID=79576.

Moghadam, M. E., Y. Bazilevs, T. Hsia, I. Vignon, A. Marsden, and T. T. M. of Congenital Hearts Alliance (2011). A comparison of outlet boundary treatments for prevention of backflow divergence with relevance to blood flow simulations. *Computational Mechanics 48*, 277–291.

Nitsche, J. (1971). Über ein variationsprinzip zur lösung von Dirichlet-problemen bei verwendung von teilräumen, die keinen randbedingungen unterworfen sind. *Abhandlungen aus dem Mathematischen Seminar der Universität Hamburg 36*, 9–15.

Porpora, A., P. Zunino, C. Vergara, and M. Piccinelli (2012). Numerical treatment of boundary conditions to replace lateral branches in hemodynamics. *International journal for numerical methods in biomedical engineering 28*, 1165–1183.

Sainte-Marie, J., D. Chapelle, R. Cimrman, and M. Sorine (2006). Modeling and estimation of the cardiac electromechanical activity. *Comput. and Struct. 84(28)*, 1743–1759.

Stenberg, R. (1995). On some techniques for approximating boundary conditions in the finite element method. *Journal of Computational and Applied Mathematics 63*, 139–148.

Tagliabue, A., L. Dedè, and A. Quarteroni (2017). Fluid dynamics of an idealized left ventricle: the extended Nitsche's method for the treatment of heart valves as mixed time varying boundary conditions. *Int. J. Num. Meth. Fluids 85*, 135–164.

Tobiska, L. and R. Verfurth (1996). Analysis of a streamline diffusion finite element method for the Stokes and Navier-Stokes equations. *SIAM Journal on Numerical Analysis 33*, 107–127.

Vignon-Clementel, I. (2006). A coupled multidomain method for computational modeling of blood flow. *PhD Thesis, Department of Mechanical Engineering, Stanford University*.

Zhou, G. and N. Saito (2016). The Navier–Stokes equations under a unilateral boundary condition of Signorini's type. *Journal of Mathematical Fluid Mechanics*.